IEEE Access
Multidisciplinary | Rapid Review | Open Access Journal

Received January 31, 2022, accepted February 12, 2022, date of publication February 22, 2022, date of current version March 2, 2022.

Digital Object Identifier 10.1109/ACCESS.2022.3153318

Improved Ground Target Detecting System Based on Both Miniaturized FMCW Radar and Radiometer

MYUNG-SUK JUNG AND KYUNG-TAE KIM, (Member, IEEE)
Department of Electrical Engineering, Pohang University of Science and Technology, Pohang 37673, South Korea
Corresponding author: Kyung-Tae Kim (kkt@postech.ac.kr)

ABSTRACT The frequency-modulated continuous-wave (FMCW) radar is generally applied in ground target detecting devices mounted on small shells or projectiles because of its compact size. However, the FMCW radar often produces false alarms when detecting ground targets surrounded by heavy clutter. To overcome this problem, this paper proposes a ground target detection system based on both the miniaturized FMCW radar and the total power radiometer (TPR), consisting of the common millimeter-wave (MMW) front ends and an antenna. However, its intermediate frequency (IF) parts are separated using different frequency bands to miniaturize the entire system. The minimum detectable temperature (MDT) increases and the sensitivity is thus degraded because the TPR for the hybrid sensor inevitably includes an undesirable transmitter section owing to the widespread usage of the front ends with the radar. The proposed system employs optimization of the physical path delay and duplexing the IF band for the TPR and FMCW radar to improve the sensitivity of the TPR in the proposed hybrid sensors and reduce the system noise. The system includes a matching circuit and a voltage doubler to improve the sensitivity of the detector. Therefore, the MDT of TPR in the proposed hybrid system can be reduced to 47.5 K from 734.6 K in the initial design. The drop test demonstrates that the proposed hybrid sensor can reduce false alarms when compared to using either the FMCW radar or only the TPR.

INDEX TERMS Detector, FMCW radar, MDT, MMW, multi-sensor, sensitivity, TPR.

I. INTRODUCTION

A frequency-modulated continuous wave (FMCW) radar mounted on a small shell or projectile can be used to detect ground targets [1]. The hardware architecture of the FMCW radar is concise and simple and can be easily miniaturized to produce compact sensors. Additionally, it can detect targets with a low radar cross-section (RCS) owing to its high sensitivity [1]. However, it often produces false alarms, especially while detecting ground targets, owing to heavy clutters such as trees, buildings, bridges, etc., whose RCS is comparable to that of the desired ground target.

For effective target detection in heavy ground clutter, the FMCW radar can be designed as a non-linear radar [2]–[6]. Because the operating frequencies of the transmitting and receiving portions of the nonlinear FMCW radar must be different, the structure of the nonlinear FMCW radar is inevitably more complicated than that of a typical FMCW radar. Therefore, the nonlinear FMCW radar is unsuitable for application in small spaces such as shells.

A sensor-fusion strategy which integrates the FMCW radar and the radiometer can be employed to reduce the number of false alarms. The radiometer can quickly respond to targets whose brightness temperature varies significantly from that of the ground. This makes it highly effective in detecting ground vehicles as they typically have a much lower brightness temperature when compared to ground clutters [7]–[9]. Therefore, radiometers applied in conjunction with the FMCW radar can improve the detection capability of ground vehicles even in the presence of heavy ground clutter, thus reducing the number of false alarms.

Several studies have proposed a hybrid system consisting of both radar and radiometer to improve the performance of the target-detecting system [10]–[16]. Some studies employed the frequency division method using a duplexer or diplexer in the radio frequency (RF) section [10], [11], where

The associate editor coordinating the review of this manuscript and approving it for publication was Chun-Hsing Li.

the FMCW radar and radiometer share the same antenna. However, such systems are too bulky and cannot be mounted on a small shell or projectile. Other approaches involved using a switch for the alternating operation of the FMCW radar and radiometer in the time domain [12], [13]. However, the simultaneous operation of both sensors is unfeasible because the radiometer usually requires a much longer integration time (i.e., a few milliseconds) when compared to the radar. Therefore, these two sensors are not time-synchronous, causing the deterioration of the detection performance, especially for time-critical missions such as the detection of targets of interest for shells and projectiles. The results of recent studies [14]–[16] demonstrated that combining the outputs of radars and radiometers mounted on satellites improved the radar detection performance. However, these works primarily involved software convergence instead of hardware convergence.

This study proposes a miniaturized hybrid sensor based on an FMCW radar and a total output radiometer (TPR), that can detect targets without errors even in the presence of ground clutters with similar or larger RCSs than the target. The proposed hybrid sensor utilizes an antenna in conjunction with the millimeter wave (MMW) front ends to miniaturize the entire system. The intermediate frequency (IF) parts are separated for the simultaneous operation of the FMCW radar and TPR at different frequencies.

The proposed system has the advantage of being smaller in size than the designs in [10]–[13] and simultaneous operation of the two sensors in contrast to those in [12], [13]. Therefore, according to the authors' knowledge, our hybrid sensor is the most compact research sensor based on FMCW and radiometer, making it possible to quickly process the fused target signals.

In the initial design, it was observed that the FMCW radar part of the sensor operates normally, but the TPR part does not. To solve this problem, the cause of the TPR failure in the initial design is analyzed in Section II, and an improved hybrid sensor is proposed based on this analysis. The proposed sensor adjusts the physical delay difference and duplexes the appropriate IF band for the TPR and FMCW radar to reduce the amount of system noise, and includes an appropriate matching circuit and voltage doubler to improve the sensitivity of the radiometer. Section III demonstrates through measurements that the sensitivity of the TPR part is improved when compared to the initial design. Furthermore, the drop test of the designed hybrid sensor demonstrates the performance of the detection of the ground vehicle surrounded by heavy clutters. Lastly, Section IV concludes the paper.

II. ANALYSIS AND DESIGN OF THE TPR IN A MINIATURIZED HYBRID SENSOR SYSTEM

A. CONVENTIONAL TPR

In the conventional TPR (Fig. 1), an IF signal is produced by combining the noise and reference signal received from the local oscillator (LO) in the mixer. The resultant IF signal is amplified by using a low-noise amplifier (LNA). The amplified signal is converted to a voltage signal proportional to the noise power in the detector. Lastly, the signal is sequentially amplified and filtered in the low-frequency amplifier and low-pass filter (LPF), respectively.

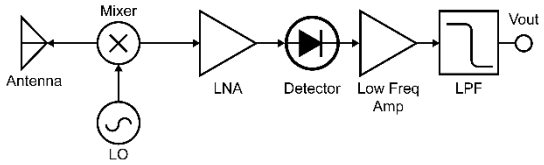

FIGURE 1. The configuration of the conventional TPR. Components and process are described in the text.

The final output, V_{out} (Fig. 1), can be obtained as follows:

$$V_{out} = G_{LF} \times S \times G_R \times P_{IN} \tag{1}$$

where G_{LF} represents the gain of the low-frequency amplifier, S denotes the sensitivity of the detector, and G_R represents the total gain of the receiver before the detector.

The equivalent input noise power of the radiometer, P_{IN}, is defined as follows:

$$P_{IN} = kT_{SYS}B \tag{2}$$

where k represents the Boltzmann's constant (i.e., 1.38×10^{-23}(J/K) and B (Hz) represents the frequency bandwidth of the system. The system temperature of the radiometer, T_{SYS}, in Kelvin is given by:

$$T_{SYS} = \eta_l(eT_{T0} + \Gamma_i T_{SKY})/L_a + (NF_R - 1)T_{S0} \tag{3}$$

where η_l denotes the antenna efficiency ($0 \leq \eta_l \leq 1$), e is the emissivity of the target ($0 \leq e \leq 1$), T_{T0}(K) is the physical temperature of the target, Γ_i is the reflection coefficient of the target, T_{SKY}(K) is the sky temperature that varies with the zenith angle, weather condition, and humidity [17], [18], L_a is the atmospheric attenuation, NF_R is the noise figure of the receiver, and T_{S0}(K) denotes the physical temperature of the receiver.

The minimum detectable temperature (MDT), i.e., the sensitivity of the radiometer, is calculated as:

$$MDT = T_{SYS}/\sqrt{B\tau} \tag{4}$$

where B (Hz) represents the frequency bandwidth of the TPR, and τ (s) represents the integration time, which is inversely proportional to the bandwidth of the LPF.

B. INITIAL DESIGN OF HYBRID SENSOR SYSTEM

Fig. 2 depicts the initial configuration of the hybrid sensor system consisting of the TPR and FMCW radar, which is used to detect ground targets with heavy clutter. The TPR part of the initial configuration includes a voltage-controlled oscillator (VCO) used with a modulation signal generator instead of the LO (shown in Fig. 1) in the MMW front-end. The coupler delivers a part of the output of the VCO to the mixer. The circulator isolates the transmitted signal

from the received signal and a divider is used to distribute the input power to the radiometer and radar. The hybrid system depicted in Fig. 2 is compact due to its common parts.

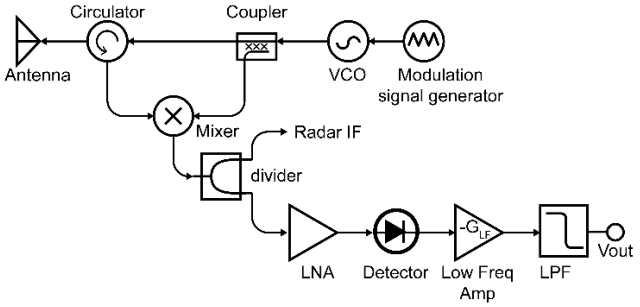

FIGURE 2. The first trial configuration of the hybrid sensor; the TPR operating simultaneously with an FMCW radar. Components and processes are described in the text.

However, the tests conducted on the initially designed hybrid sensor system demonstrate that the FMCW radar part operates normally, while the TPR part does not. The TPR part only operates normally when the path between the circulator and coupler is removed (i.e., TPR-only operating state). It is assumed that the MDT of the TPR (i.e., sensitivity) is significantly deteriorated by the noise added by the transmission part of the FMCW radar.

Therefore, the amount of additional noise added due to the transmitter part of the FMCW radar is analyzed by using the system noise equations of the FMCW radar in [19] and [20]. The noise is generated due to the correlation between the phase noise of the leakage signal of the VCO and the signal of the LO in the mixer output. The correlation factor, K^2, is as follows [19], [20]:

$$K^2 = 2(1 - \cos(2\pi ft)) \tag{5}$$

where f (Hz) represents the offset frequency from the transmitting carrier (IF frequency) and t (s) represents the difference in the delay between the LO and the leakage path. K^2 increases with the increase in t at f lower than approximately 1 GHz, and K^2 does not depend on the delay difference, t, at f higher than approximately 1 GHz (Fig. 3).

The configuration of the TPR in the hybrid system presented in Fig. 2 has two significant leakage paths (Fig. 4): path (1), on which the output of the VCO is reflected by the antenna and then passes through the RF input of the mixer, and path (2), on which the VCO output is present in the RX port of the circulator owing to the limited performance in isolation and then passes through the RF input of the mixer.

If the phase noise of the VCO is $PN(f)$ at any f, the equivalent noise power, P_{Mixer}, in the mixer's output, including the noise, $P_{N(1)}$ and $P_{N(2)}$, added by both the leakage paths, (1) and (2), is:

$$P_{Mixer} = P_{IN} - L_R + P_{N(1)} + P_{N(2)} \tag{6}$$

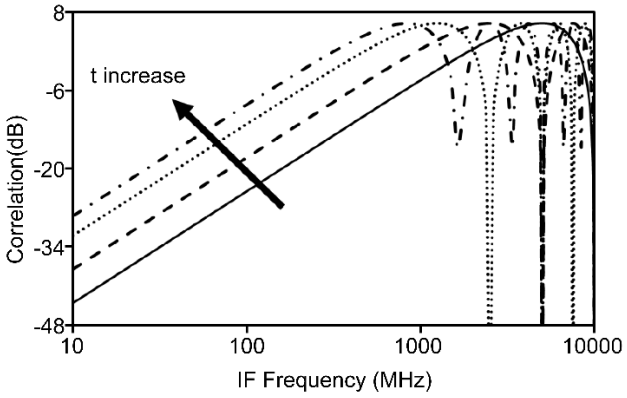

FIGURE 3. K^2 of the phase noise based on five t values: t = 100 ps (solid line), 200 ps (dashed line), 400 ps (dotted line), and 600 ps (dashed-dotted line).

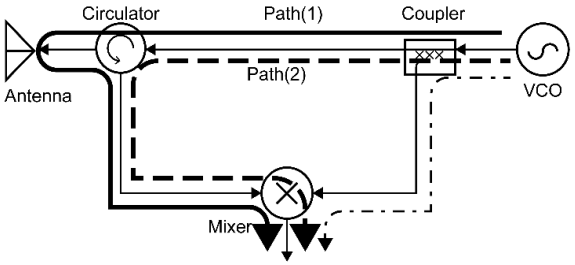

FIGURE 4. Two significant leakage paths: Path (1) (solid line): VCO – coupler - circulator – returned by antenna – circulator – mixer; Path (2) (dashed line): VCO – coupler -circulator – mixer.

where L_R (dB) represents the loss of the receiver from the antenna to the mixer.

$$P_{N(n)} = PN(f) + K^2_{(n)} + P_{(n)} \text{ (n = 1, 2)} \tag{7}$$
$$P_{(1)} = P_t - IL_c - IL_{cir-TX} - \Gamma_A - IL_{cir-RX} \tag{8}$$
$$P_{(2)} = P_t - IL_c - ISO_{cir} \tag{9}$$

where $K^2_{(n)}$ is K^2 in each leakage path ($n = 1, 2$), $P_{(n)}$ is the leakage power in each leakage path ($n = 1, 2$), P_t (dBm) represents the output power of the VCO, IL_c(dB) is the insertion loss of the coupler, IL_{cir-TX} (dB) is the insertion loss in the transmission path of the circulator, Γ_A (dB) is the reflection coefficient of the antenna, IL_{cir-RX} (dB) is the insertion loss in the receiving path of the circulator, and $ISO_{cir-ISO}$ (dB) represents the isolation of the circulator.

Using (6) and (2), the equivalent system noise temperature T'_{SYS} can be given as:

$$T'_{SYS} = T_{SYS} + T_{E(1)} + T_{E(2)} \tag{10}$$
$$T_{E(n)} = P_{N(n)}/kB, (n = 1, 2). \tag{11}$$

From (4) and (10), the MDT of this new configuration is given by:

$$MDT' = T'_{SYS}/\sqrt{B\tau}. \tag{12}$$

Therefore, the MDT of this configuration increases due to $T_{E(1)}$ and $T_{E(2)}$ and the sensitivity of the TPR is thus significantly degraded.

The fabricated TPR in the initial design had $T'_{SYS} =$ 464,618 K and $MDT' = 734.6$ K at 100 MHz using (10) and (12). If the TPR had only receiving parts as the conventional radiometer, T_{SYS} would be 6,663 K and MDT would be 10.5 K at 100 MHz using (3) and (4).

These results indicate that the TPR cannot work because of the unwanted noise caused by the transmitter part of the FMCW radar. The physical path delay difference of each path must be reduced to minimize the $K^2_{(n)}$ value, and/or the absolute leakage noise level, $P_{(n)}$, must be minimized to solve this problem. Reducing $P_{(n)}$ faces a limitation in practical conditions because of the finite reflection coefficient of the antenna and the isolation characteristics of the circulator. However, the physical path difference can be adjusted to determine its effect.

C. VERIFICATION EXPERIMENTS

The validity of the above analysis is verified using the prototype of the hybrid sensor system shown in Fig. 5. Waveguide components are employed to adjust the physical path delay of the two points.

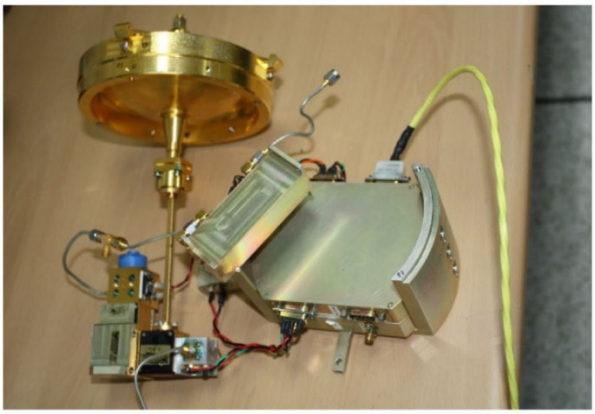

FIGURE 5. Experimental configuration using the prototype of the hybrid sensor.

The noise level is measured at 100 MHz using a spectrum analyzer at the IF output port of the mixer, as shown in Fig. 6.

In experiment 1, SWG1 (standard waveguide) is inserted into the antenna path of the reference case (REF), but the noise level does not increase. $P_{(1)}$ in (8) is almost identical to that in the REF case owing to a dominant component of

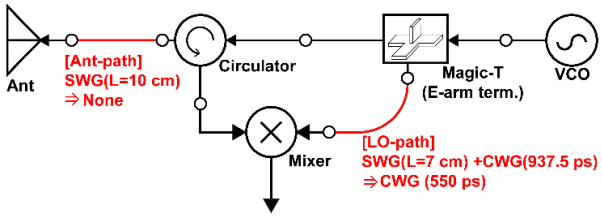

FIGURE 6. Test condition of validation experiments.

TABLE 1. Test result of validation experiments.

Case	Ant-path	LO-path	Noise level [dBm]	
			Calculated	Measured
REF	None	CWG1 (550 ps)	-65.87	-66.7
Exp1.	SWG1 (436 ps)	CWG1 (550 ps)	-65.21	-66.8
Exp2.	None	SWG2 + CWG2 (1239 ps)	-56.42	-56.0

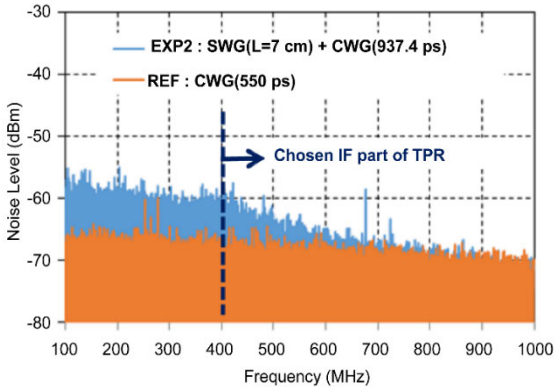

FIGURE 7. Test results; noise level at RBW (resolution bandwidth) of 30 kHz: Exp2 (blue line), REF (red line).

Γ_A at the output of the circulator. In experiment 2, CWG1 (custom waveguide) on the LO path in REF, is replaced with SWG2 and CWG2, and the noise level increased by approximately 10 dB, as shown in Fig. 7. It can be observed from Table 1 that the calculated noise power, obtained by using (6), concurs well with the measured noise power. The experiment demonstrates the effect of the variation of the LO path delay on $K^2_{(n)}$ and the noise power, $P_{N(n)}$, of the sensor.

D. PROPOSED HYBRID SENSOR SYSTEM

A new hybrid sensor system is proposed based on the above description to accurately apply the TPR part of the initial configuration, as shown in Fig. 8.

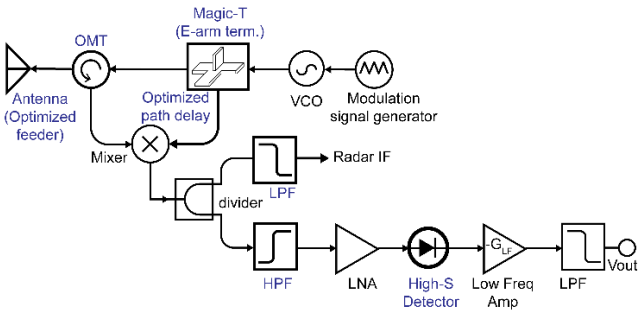

FIGURE 8. The proposed configuration of the hybrid sensor; the TPR operating simultaneously operating a FMCW radar. Components and processes are described in the text.

The unwanted noise due to the transmitter part is decreased by optimizing the feeder length of the antenna and the physical path delay between the coupler and mixer. Additionally, the size of the system is reduced significantly by exchanging a circulator and a coupler to an orthomode

transducer (OMT) and E-arm terminated magic-T. Subsequently, filters are utilized to separate the radiometer signal from the unwanted noise signal owing to the radar signal. Therefore, the sensitivity of the detector is improved to compensate for this degradation in the sensitivity of the TPR.

The feeder length of a Cassegrain antenna and the physical length of the path between the coupler and mixer is optimized to decrease the unwanted noise due to the transmitter part. However, there is a lower limit in reducing the physical owing due to the structural limitations of the MMW front-end. Therefore, the circulator in the initial configuration is replaced with an orthomode transducer (OMT) to improve the isolation capability between the TX and RX parts by +4 dB. Additionally, the size of the coupler in the initial configuration is reduced by using E-arm terminated magic-T in the MMW front-end.

A high-pass filter (HPF) is used between the divider and LNA in the TPR, and the cut-off frequency of the HPF is set to 400 MHz considering the noise level in Fig. 7, to separate the radiometer signal from the radar signal.

Furthermore, a low-pass filter (LPF) with a cut-off frequency of 2 MHz is used for the radar-IF part. Therefore, the unwanted phase noise derived from the VCO can be suppressed in both the radar and the TPR parts.

A diode detector consisting of a voltage doubler and a matching circuit is proposed to further improve the sensitivity of the TPR, as shown in Fig. 9. The matching circuit can operate between 400 MHz and 700 MHz to ensure the rejection of phase noise in the TPR under 400 MHz and interference from the wireless communications over 800 MHz.

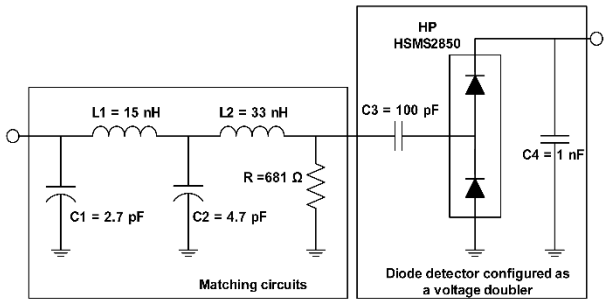

FIGURE 9. The detector using a voltage doubler and matching circuit. C1206 series multilayer ceramic capacitors (Kemet) was used in C1 and C2, IC1210 series SMT inductors (ACT) was used in L1 and L2 and the thick film chip resistor (Vishay Dale) was used in R.

It can be observed from Fig. 10, that when the detector uses only a single diode without a matching circuit, its sensitivity is 3.4 mV/μW (dashed line) according to the simulations conducted by the Advanced Design System (ADS^{TM}). Similarly, the sensitivity of the proposed detector with two diodes and a matching circuit lies between 8 mV μW and 12 mV/ μW within the 400–700 MHz frequency band (Fig. 10, solid line). It can be observed by comparing the dashed and solid lines in Fig. 10, that the sensitivity of the proposed detector is improved by approximately 3.5 times at 600 MHz.

Additionally, the measurement result of the proposed detector is indicated by a dotted line in Fig. 10, and

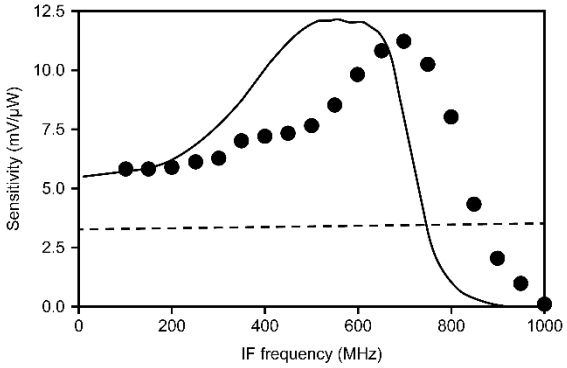

FIGURE 10. Sensitivity of the detector; solid line: the simulated sensitivity, dashed line: a single diode detector without matching circuit, dotted line: measured sensitivity of proposed detector.

the sensitivity of the fabricated detector is 11.2 mV/ μW at 700 MHz, which is similar to that in the simulation. The maximum peak of the sensitivity is shifted by approximately 100 MHz when compared to the simulation, due to the tolerance of the components used in the matching circuit; however, they both have similar trends against the IF frequency.

III. EXPERIMENT RESULT

A. SENSITIVITY MEASUREMENT OF PROPOSED HYBRID SENSOR

The proposed hybrid sensor is fabricated by using a Cassegrain antenna, an integrated MMW front-end, and a miniaturized IF/power part, as shown in Fig. 11. The parameters in the TPR part are measured to calculate T'_{SYS} and MDT' of the fabricated hybrid sensor, as shown in Table 2 and Fig. 12.

TABLE 2. Measured parameters in the TPR part of the hybrid system.

Parameter	Unit	Initial Design	Proposed Design
P_t	dBm	+15.97	+15.40
NF_R	dB	+13.61	+10.25
G_R.	dB	+33.89	+40.25
T_{SYS}	K	6,663	1,317
$T_{E(1)}$	K	166,990	28,053
$T_{E(2)}$	K	290,965	643
T'_{SYS}	K	464,618	30,013
MDT'	K	734.6	47.5

$T_{E(1)}$ can be reduced from 166,990 K (initial design) to 28,053 K (proposed design) and $T_{E(2)}$ from 290,965 K (initial design) to 643 K (proposed design) by optimizing the physical length of the feeder and the LO path. However, it is observed that there is a lower limit to reduce the amount of leakage noise by adjusting the physical path delay because there are several reflection paths of the antenna, as shown in Fig. 12.

The fabricated TPR in the proposed hybrid system has $T'_{SYS} = 30{,}013$ K and $MDT' = 47.5$ K at 700 MHz using (10) and (12). The improvement in the sensitivity of the detector is considered while calculating the T'_{SYS} and MDT' values.

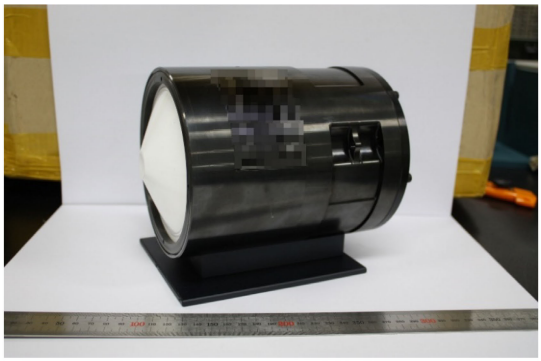

(a) Full configuration

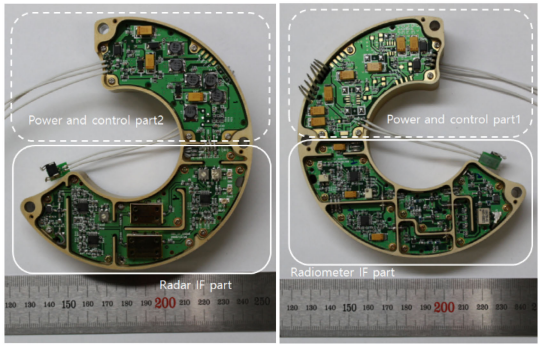

(b) IF parts of the hybrid sensor: top view (left): bottom view (right).

FIGURE 11. The fabricated hybrid sensor based on miniaturized FMCW radar and TPR.

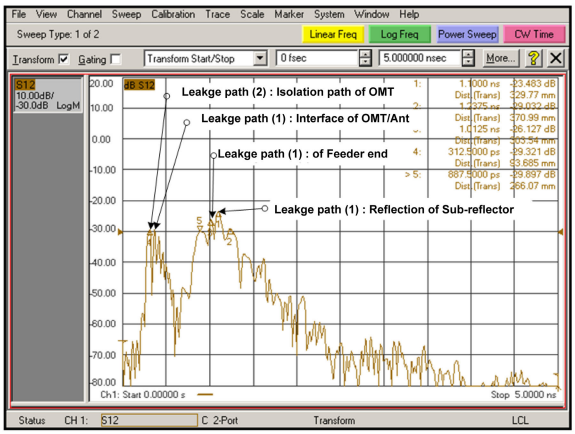

FIGURE 12. Measured leakage path delay of OMT + Cassegrain antenna of the final made hybrid (with jig delay, 200 ps).

Based on these results, it can be observed that the sensitivity of the proposed hybrid system is improved from 734.6 K to 47.5 K, which is a significant enhancement when compared to the initial design.

B. SENSOR SYSTEM EXPERIMENT

The performance of the ground target detection system is evaluated by using the proposed hybrid sensor system which comprises the TPR and the FMCW radar. The hybrid sensor system is dropped from a helicopter at a height of 300 m above the ground. Fig. 13 presents the measurement setup, including the ground vehicle to be detected, the helicopter, and the hybrid sensor system. The ground below

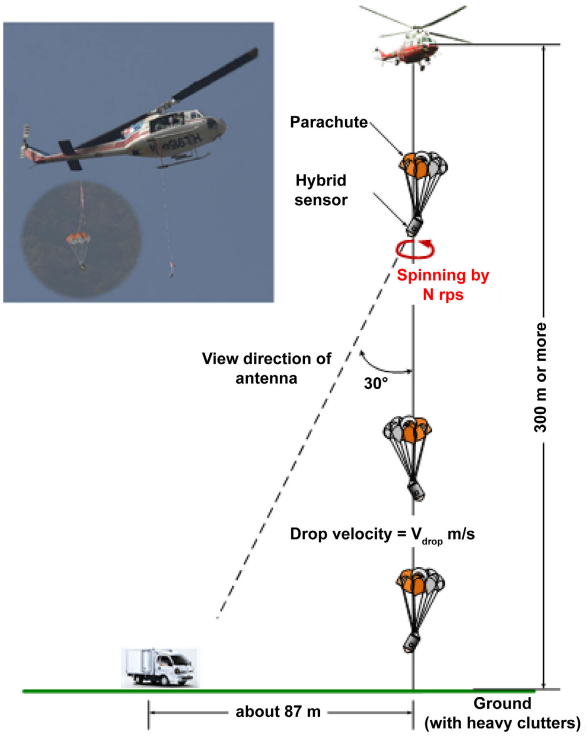

FIGURE 13. Conditions for the drop test of the hybrid sensor.

the helicopter includes heavy clutters, such as concrete roads and waterways, small buildings, soil, small trees, and rocks.

The envelope (magnitude of beat signals) and the magnitude of the output of the TPR is recorded by using a storage device in a hybrid sensor. The hybrid sensor is dropped and rotated around a certain axis at a constant speed, using a specially designed parachute, as shown in Fig. 13. Following the ground collision, the results of the storage device in the hybrid sensor are presented in Fig. 14(a).

The proposed ground detection system determines the presence of ground vehicles by comparing the outcomes of the FMCW radar and the TPR. Particularly, the hits (i.e., detected peaks above the threshold level) of the FMCW radar and those of the TPR are integrated to determine the existence and location of a target. The information of the hits can be obtained by using a conventional constant false alarm rate (CFAR) detection algorithm. The existence and location of the desired target is declared only when two peaks from the FMCW radar and TPR are detected at the same instant (i.e., range).

In Fig. 14 (a), the upper figure depicts the envelope of the beat signal in the FMCW radar, and the lower figure depicts the magnitude of V_{out} in the TPR. There are a large number of peaks in both the FMCW radar and TPR owing to heavy clutter, as shown in Fig. 14 (a). Especially in the case of the FMCW radar, the target cannot be discriminated from the surrounding clutter because the response due to the clutter is significantly higher than the response due to the target. Conversely, the TPR presents a clear target response when

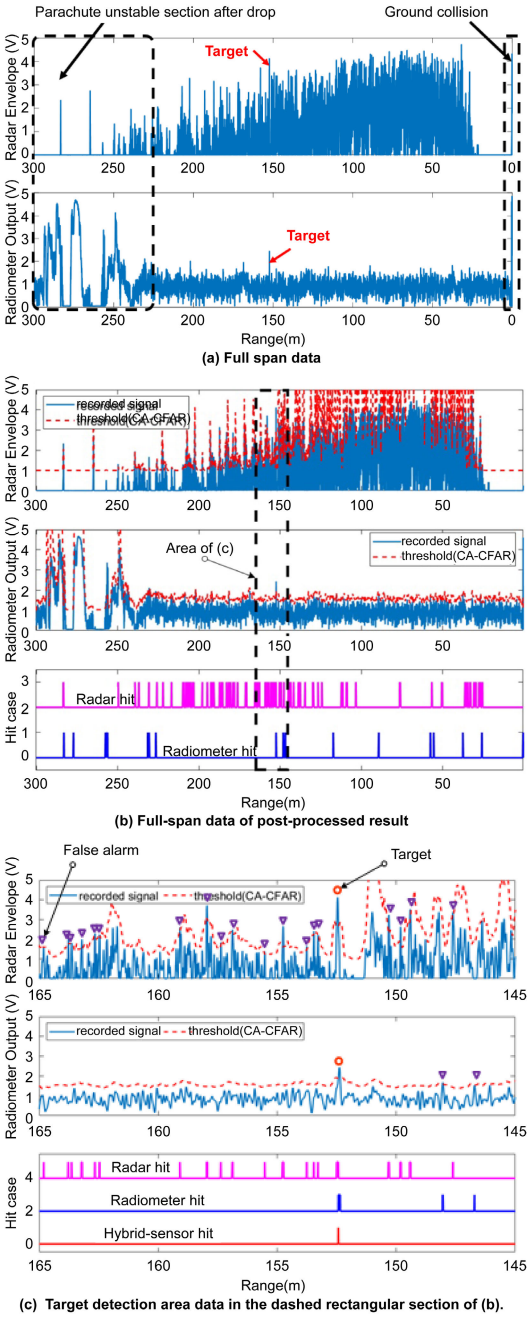

FIGURE 14. Results of the drop test.

compared to the FMCW radar because of the improvement of MDT' in the proposed hybrid sensor system.

In Fig. 14 (b), the uppermost figure presents the threshold (red-dashed line) for the FMCW radar obtained by CA-CFAR (Cell Averaging – CFAR) detection algorithm, and the middle figure presents the threshold (red-dashed line) for the TPR.

The threshold of the CA-CFAR detector shown in Fig. 14 (b) is obtained by using numerous reference cells (N) of 256, and the desired probability of false alarm (P_{FA}) of 10^{-4} for the FMCW radar. Conversely, for TPR, the P_{FA} is set to 10^{-2} with the same $N = 256$. Neither the FMCW radar nor the TPR can discriminate between the desired ground vehicle and the various ground clutters. The TPR section of the proposed hybrid sensor produced a few false alarms owing to surrounding clutters despite the significant improvement produced by optimizing the physical delay, and utilizing a dedicated high-sensitivity detector. However, the TPR part did not function at all in the initial design due to the unwanted noise from the FMCW radar part. Conversely, the proposed TPR in the hybrid sensor can detect targets as well as some surrounding clutters, as shown in the middle figure of Fig. 14 (b).

The detection results of both the FMCW radar and TPR are presented in the lowermost figure of Fig. 14 (b). It is observed that the number of hits for the FMCW radar is equal to 100 (i.e., the number of false alarms is 99), while that for TPR is 23 (i.e., the number of false alarms is 22).

Fig. 14 (c) presents a magnified view of the inner part of the rectangle (dashed line) in Fig. 14 (b). The lowermost figure in Fig. 14 (c) presents the final detection result (red solid line) obtained by using the results (magenta solid line) of the FMCW radar and those (blue solid line) of the TPR. The presence of a ground vehicle is declared when the detection results of the FMCW radar and TPR lie within the same range bin, presenting a single peak without any false alarms due to the surrounding heavy clutters.

C. DISCUSSION

It is observed from the sensitivity measurement, that the unwanted noise due to the transmitter part (i.e., $T_{E(n)}$) is reduced by optimizing the physical length of the feeder and the LO path and by replacing the circulator and the coupler with an orthomode transducer (OMT) and an E-arm terminated magic-T, respectively. The sensitivity of TPR in the proposed hybrid system (i.e., MDT') is improved from 734.6 K to 47.5 K.

The sensitivity of the detector is improved by applying an appropriate matching circuit and voltage doubler configuration in the TPR.

The drop test experiment demonstrates that the proposed hybrid sensor can effectively detect ground vehicles even in the presence of heavy ground clutter. The performance of the proposed hybrid sensor is significantly improved in conjunction with the specially designed TPR despite the high false alarm rate of the FMCW radar due to heavy ground clutter. Therefore, the desired ground target is successfully detected without any false alarms.

It should be noted that, to lower the probability of erroneous detection in our proposed target detection system, the radiometer operation is critical. Because radiometers are more affected by weather conditions than FMCW radars in the W-band, the performance of the proposed system may deteriorate, particularly in bad weather conditions, e.g., heavy rain.

IV. CONCLUSION

This study proposes a hybrid sensor based on both the miniaturized FMCW radar and TPR to detect vehicles in the

presence of heavy ground clutter. The hybrid sensor applied the MMW front end and an antenna of the FMCW radar as is, and used only the IF part with different frequency bands for each system to reduce the size of the entire system. The TPR did not work in this initial configuration because the MDT of the TPR increased due to additional noise produced by unnecessary transmission parts of the TPR. The effect of the physical path delay difference was analyzed to ensure the effective working of the TPR in the proposed hybrid sensor. The delays were optimized based on the analysis to minimize the phase noise inflow path of the VCO, which causes the noise, and the IF band of the TPR was selected considering the frequency characteristic of the incoming noise. Additionally, an appropriate matching circuit and voltage doubler configuration were applied in the TPR to improve the sensitivity of the detector. The MDT of TPR in the proposed hybrid system can be reduced from 734.6 K in the initial design, to 47.5 K. While this 47.5 K value is too high for a system that requires target discrimination such as a precise image sensor, it is considered a valid value for the operation of the hybrid system proposed in this paper. The effectiveness of the designed hybrid sensor system, which was mounted on a shell, to detect ground vehicles was demonstrated by a drop test. This experiment demonstrated the proposed ground target detection system's ability to detect and discriminate desired ground targets, even with many false alarms produced by heavy ground clutter.

In future, we plan to develop a more compact and low-cost hybrid sensor by applying a CMOS-based MMW front end.

ACKNOWLEDGMENT

The authors would like to thank Editage (www.editage.co.kr) for English language editing.

REFERENCES

[1] M. I. Skolnik, *Introduction to Radar Systems*, 2nd ed. New York, NY, USA: McGraw-Hill, 1981.
[2] J. Shefer and R. J. Klensch, "Harmonic radar helps autos avoid collisions," *IEEE Spectr.*, vol. 10, no. 5, pp. 38–45, May 1973.
[3] R. Hstger, "Harmonic radar systems for near-ground in-foliage nonlinear scatterers," *IEEE Trans. Aerosp. Electron. Syst.*, vol. AES-12, no. 2, pp. 230–245, Mar. 1976.
[4] F. Crowne and C. Fazi, "Nonlinear radar signatures from metal surfaces," in *Proc. Int. Radar Conf. Surveill. Safer World (RADAR)*, 2009, pp. 1–6.
[5] G. J. Mazzaro, A. F. Martone, K. I. Ranney, and R. M. Narayanan, "Nonlinear radar for finding RF electronics: System design and recent advancements," *IEEE Trans. Microw. Theory Techn.*, vol. 65, no. 5, pp. 1716–1726, May 2017.
[6] G. J. Mazzaro, K. A. Gallagher, K. D. Sherbondy, and A. F. Martone, "Nonlinear radar: A historical overview and a summary of recent advancements," *Proc. SPIE*, vol. 11408, May 2020, Art. no. 114080E.
[7] F. T. Ulaby, R. K. Moore, A. K. Fung, and D. S. Simonett, *Microwave Remote Sensing: Active and Passive: Fundamentals and Radiometry*, vol. 1. Reading, MA, USA: Addison-Wesley, 1981.
[8] N. Skou, *Microwave Radiometer Systems: Design & Analysis*. Norwood, MA, USA: Artech House, 1989.
[9] G. Evans and C. W. McLeish, *RF Radiometer Handbook*. Norwood, MA, USA: Artech House, 1977.
[10] D. Huddleston, J. Savage, B. Sundston, B. Belcher, and D. Ewen, "Radarometer sensor simultaneous active and passive imaging using a common antenna," *Proc. SPIE*, vol. 3703, pp. 33–44, Apr. 1999.
[11] D. Ewen, D. Huddleston, R. Smith, and B. Belcher, "Flight test of a MMW imaging radarometer," *Proc. SPIE*, vol. 4373, pp. 22–34, Aug. 2001.
[12] A. K. Arakelyan, "Microwave Doppler radar and radiometer system for spatial-time-combined observation of targets," *Proc. SPIE*, vol. 4129, pp. 535–542, Jul. 2000.
[13] D. G. Macfarlane, H. M. Odbert, D. A. Robertson, M. R. James, H. Pinkerton, and G. Wadge, "Topographic and thermal mapping of volcanic terrain using the AVTIS ground-based 94-GHz dual-mode radar/radiometric imager," *IEEE Trans. Geosci. Remote Sens.*, vol. 51, no. 1, pp. 455–472, Jan. 2013.
[14] J. H. Jiang, Q. Yue, H. Su, P. Kangaslahti, M. Lebsock, S. Reising, M. Schoeberl, L. Wu, and R. L. Herman, "Simulation of remote sensing of clouds and humidity from space using a combined platform of radar and multifrequency microwave radiometers," *Earth Space Sci.*, vol. 6, no. 7, pp. 1234–1243, Jul. 2019.
[15] M. Montopoli, D. Cimini, E. Picciotti, S. Di Fabio, V. Capozzi, K. De Sanctis, and F. S. Marzano, "Investigating ground-based radar and spaceborne infrared radiometer synergy for lightning areal prediction in complex orography," *Bull. Atmos. Sci. Technol.*, vol. 1, no. 2, pp. 231–256, Jul. 2020.
[16] S. Schnitt, U. Löhnert, and R. Preusker, "Potential of dual-frequency radar and microwave radiometer synergy for water vapor profiling in the cloudy trade wind environment," *J. Atmos. Ocean. Technol.*, vol. 37, no. 11, pp. 1973–1986, Nov. 2020.
[17] C. R. Seashore, "Millimeter wave guidance application: An overview," *Proc. SPIE*, vol. 423, pp. 66–73, Oct. 1983.
[18] P. Bartia and I. Bahl, *Millimeter Wave Engineering and Applications*. Hoboken, NJ, USA: Wiley, 1994.
[19] J. A. Scheer and J. L. Kurtz, *Coherent Radar Performance Estimation*, Boston, MA, USA: Artech House, 1993, ch. 12.
[20] S. Goldman, "Oscillator phase noise proves important to pulse-Doppler radar systems," Microw. Syst. News, Feb. 1984, pp. 88–100.

MYUNG-SUK JUNG received the B.S. degree in electronics and electrical engineering from Kyungpook National University, Daegu, South Korea, in 1999, and the M.S. degree in electronics and electrical engineering from the Pohang University of Science and Technology (POSTECH), Pohang, South Korea, in 2001, where she is currently pursuing the Ph.D. degree.

She has been a Principal Researcher with Agency for Defense Development, Daejeon, South Korea, since 2001. Her current research interests include development of the microwave and millimeter-wave sensors.

KYUNG-TAE KIM (Member, IEEE) received the B.S., M.S., and Ph.D. degrees from the Pohang University of Science and Technology (POSTECH), Pohang, South Korea, in 1994, 1996, and 1999, respectively, all in electrical engineering. From 2002 to 2010, he was a Faculty Member with the Department of Electronic Engineering, Yeungnam University, South Korea. From 2012 to 2017, he worked as the Director of the Sensor Target Recognition Laboratory, sponsored by the Defense Acquisition Program Administration and Agency for Defense Development. Since 2011, he has been with the Department of Electrical Engineering, POSTECH, where he is currently working as a Professor. He is also the Director of the Next Generation Defense Multidisciplinary Technology Research Center, and the Next Generation Imaging Radar System Research Center, POSTECH. He is the author of approximately 300 papers in journals and conference proceedings. His research interests include primarily in the field of intelligent radar systems and signal processing, such as SAR/ISAR imaging, target recognition, direction of arrival estimation, micro-doppler analysis, automotive radars, digital beamforming, electronic warfare, electromagnetic scattering, and indoor monitoring of individuals. He was a recipient of several outstanding research and best paper awards from the Korea Institute of Electromagnetic Engineering and Science (KIEES), and international conferences. He is currently working on several research projects funded by the Korean Government and several industries.